NIH Public Access
Author Manuscript
Biomaterials. Author manuscript; available in PMC 2014 December 01.

Published in final edited form as:
Biomaterials. 2013 December ; 34(38): 10209–10216. doi:10.1016/j.biomaterials.2013.08.076.

Microdistribution of MC1R-targeted polyplexes in murine melanoma tumor tissue

Mikhail O Durymanov[1,2], **Tatiana A Slastnikova, PhD**[1], **Alexey I Kuzmich**[4], **Yuri V Khramtsov, PhD**[1,5], **Alexey V Ulasov, PhD**[1,5], **Andrey A1 Rosenkranz, PhD**[1,2,5], **Sergey Y Egorov, PhD**[6], **Eugene D Sverdlov, PhD**[3,4], and **Alexander S Sobolev, PhD**[1,2]

[1]Laboratory of Molecular Genetics of Intracellular Transport, Institute of Gene Biology, Russian Academy of Sciences, 34/5, Vavilov St., 199334, Moscow, Russia

[2]Department of Biophysics, Faculty of Biology, Moscow State University, 1-12, Leninskie Gory, 119991, Moscow, Russia

[3]Oncogenomics Group, Institute of Molecular Genetics, Russian Academy of Sciences, 2, Kurchatov Sq., 123182, Moscow, Russia

[4]Department of Genomics and Postgenomic Technologies, Shemyakin-Ovchinnikov Institute of Bioorganic Chemistry, Russian Academy of Sciences, GSP-7, 16/10, Miklukho-Maklaya, 117997, Moscow, Russia

[5]Targeted delivery of pharmaceuticals "Translek" LLC, 34/5, Vavilov St., 199334, Moscow, Russia

[6]Department of Physicochemical Biology, Faculty of Biology, Moscow State University, 1-12, Leninskie Gory, 119991, Moscow, Russia.

Abstract

Targeted sodium-iodide symporter (NIS) gene transfer can be considered as a promising approach for diagnostics of specific types of cancer. For this purpose we used targeted polyplexes based on PEI–PEG–MC1SP block-copolymer containing MC1SP-peptide, a ligand specific for melanocortin receptor-1 (MC1R) overexpressed on melanoma cells. Targeted polyplexes demonstrated enhanced *NIS* gene transfer compared to non-targeted (lacking MC1SP) ones *in vitro*. Using dorsal skinfold chamber and intravital microscopy we evaluated accumulation and microdistribution of quantum dot-labeled polyplexes in tumor and normal subcutaneous tissues up to 4 hours after intravenous injection. Polyplexes demonstrated significantly higher total accumulation in tumor tissue in comparison with subcutaneous ones (control). Targeted and non-targeted polyplexes extravasated and penetrated into the tumor tissue up to 20 μm from the vessel walls. In contrast, in normal subcutaneous tissue polyplexes penetrated less than 5 μm from the vessel walls with the level of extravasated polyplexes 400-fold less than in tumor. Accumulated polyplexes in tumor tissue caused *NIS* gene expression. Subsequent $^{123}I^-$ intravenous injection

© 2013 Elsevier Ltd. All rights reserved

Correspondence: Dr. Alexander S Sobolev, Department of Molecular Genetics of Intracellular Transport, Institute of Gene Biology, 34/5, Vavilov St., 199334, Moscow, Russia. Phone number: +7 (499) 135-31-00 Fax number: +7 (499) 135-41-05 sobolev@igb.ac.ru. mdurymanov@gmail.comslacya@gmail.comakrubik@gmail.comykhram2000@mail.rual.ulasov@gmail.comaar@igb.ac.ruegorov.msu@gmail.comedsverd@gmail.com.

Publisher's Disclaimer: This is a PDF file of an unedited manuscript that has been accepted for publication. As a service to our customers we are providing this early version of the manuscript. The manuscript will undergo copyediting, typesetting, and review of the resulting proof before it is published in its final citable form. Please note that during the production process errors may be discovered which could affect the content, and all legal disclaimers that apply to the journal pertain.

NIH-PA Author Manuscript
NIH-PA Author Manuscript
NIH-PA Author Manuscript

resulted in 6.8 ± 1.1 and 4.5 ± 0.8 % ID/g ($p < 0.001$) iodide accumulation in tumors in the case of targeted and non-targeted polyplexes, respectively, as was shown using SPECT/CT.

1. Introduction

Targeted gene delivery has a high potential for medical applications aimed therapy and early non-invasive diagnostics of cancer. There are a variety of vectors (or gene carriers) and strategies of targeted gene delivery. These gene carriers are nanoparticles with sizes ranged from several dozen to several hundred nanometers. As all nanoparticles and macromolecules, they are able to unspecific accumulation in tumor ("passive targeting") owing to "enhanced permeability and retention" (EPR) effect [1]. This effect is caused by increased uptake of macromolecules by solid tumors that can occur mainly due to a combination of poor lymphatic drainage and increased vascular permeability present within the tumor microenvironment [2, 3, 4]. Indeed, vascular tumor endothelium is disorganized with large fenestrations up to 600 nm and even more whereas in most of normal tissues the size of fenestrae does not exceed 5-12 nm [5]. In drug delivery to solid tumors, passive targeting is usually achieved using an appropriate particle size that allows selective extravasation into the tumor interstitial fluid due to increased vascular permeability of the tumor vasculature. On the other hand, drug targeting approaches tend to increase cellular internalization of the drug. Targeting of nanomedicines with a specific ligand to over-expressed receptors on the surface of cancer cells ("active targeting") is one of the most commonly used approach for targeted delivery of therapeutic vehicles [6, 7, 8]. This approach was applied for polyplexes by their targeting with a ligand to α(v)β(3) integrin receptors [9], receptors for epidermal growth factor [10], transferrin [11], folate [12], *etc*. There are some factors (e.g. high cell density, high interstitial fluid pressure in tumor) impeding extravasation and penetration of nanomedicines into tumor interstitium that significantly decrease observed therapeutic effect [13]. There are several ways to overcome penetration barrier and improve intratumoral distribution [14], some of them have clinical records [15]. Eventually, the issue about impact of extravasation and penetration factors on efficacy of gene delivery in particular with targeted and non-targeted polyplexes still remains open.

One of the most promising approaches for cancer therapy and diagnostics is Na^+,I^--symporter (NIS) gene transfer. In recent years the application of the *NIS* gene delivery and associated radiotracers as a reporter system for imaging gene expression aimed cancer diagnostics has reached the clinical trials [16]. NIS is an integral plasma membrane protein that provides active accumulation of iodide in several tissues of mammals including thyroid, salivary glands, gastric and rectal mucosa and the lactating mammary glands [17]. Owing to ability of NIS to transport iodide as well as pertechnetate, perrhenate and astatine, *NIS* gene delivery is very promising strategy for both diagnostics (^{99m}Tc, ^{123}I, ^{124}I, ^{125}I) and radiotherapy (^{131}I, ^{211}At, ^{188}Re, ^{186}Re) of cancer [18]. There are many studies demonstrating feasibility of *NIS* gene transfer for ectopic expression (i.e. in tumors) using both viral [19, 20] and non-viral vectors [21, 22].

The current study aimed evaluation of the potential of polyethylenimine-polyethylenglycol (PEI-PEG)-based polyplexes targeted with the synthetic MC1SP-peptide, a ligand highly specific for melanocortin receptor-1, for diagnostics of murine melanomas using small-animal single photon emission computed tomography/X-ray computer tomography (SPECT/CT) and *NIS* as a reporter gene. Earlier we showed the advantage of MC1SP-targeted polyplexes for therapeutic gene transfer in murine melanoma tumors after local administration in comparison with non-targeted ones [23].

NIH-PA Author Manuscript NIH-PA Author Manuscript NIH-PA Author Manuscript

NIH-PA Author Manuscript
NIH-PA Author Manuscript
NIH-PA Author Manuscript

We also aimed to clarify the processes of polyplex accumulation, extravasation and penetration into tumor tissue using dorsal skinfold chamber and intravital confocal microscopy. We hope that our data will make it possible to find new approaches for improvement of polyplex-mediated *NIS* gene transfer resulted in enhancement of radioisotope accumulation in tumor.

2. Materials and Methods

2.1. Polymers and plasmids

Block-copolymers of linear 25 kDa polyethylenimine (PEI) (Polysciences, Warrington, PA), and heterobifunctional polyethylene glycol MAL-dPEG24™-NHS ester (PEG) (Quanta BioDesign, Powell, OH), were synthetized as described previously [23]. On the next step, MC1SP-oligopeptide CGYGPKKKRKVSGSGSSIISHFRWGKPV (Rusbiolink, Moscow, Russia) was covalently attached to the PEI–PEG block-copolymer [23].

pCMV-NIS, pEGFP-N1 (Clontech, Mountain View, CA) and pGL3-BV (Promega, Madison, WI) encoding rat sodium-iodine symporter under cytomegalovirus immediate early promoter (CMV), enhanced green fluorescence protein under the same promoter and firefly luciferase without promoter, respectively, were propagated in *Escherichia coli* (DH5α), purified by EndoFree Plasmid Maxi or Giga Kit (Qiagen, Hilden, Germany), and stored at – 40 °C.

For obtaining of pCMV-NIS vector full-length open reading frame (ORF) rNIS was cloned from thyroid cDNA of *Rattus norvegicus*. cDNA fragment (1857 bp) corresponding to the full-length ORF of rNIS (NCBI Reference Sequence: NM_052983.2) was amplified using two primers (5'-CCACCATGGAGGGTGCGGAGGC-3' and 5'-CGGTACCCTCAGAGGTTGGTCTCCA-3'). The forward primer was designed to introduce a Kozak sequence. PCR reaction was performed using the Encyclo PCR Kit (Evrogen, Moscow, Russia). PCR product was purified, cloned into the pAL-TA plasmid (Evrogen) and sequenced. On the next step, EcoRI-EcoRI fragment carrying ORF rNIS was excised and cloned into pGL3-pCMV-FCU1 vector [24] in place of FCU1 fusion gene.

Labeling of plasmid DNA with QD605 quantum dots ITK Streptavidin Conjugate (Invitrogen/Molecular Probes, Eugene, OR) for experiments with intravital microscopy was performed as described earlier [23, 25].

2.2. Preparation of polyplexes

Polyplexes were prepared in sterile buffer solution (5% D-glucose, 5 mM HEPES, pH 7.4). Briefly, the polymer solution was added rapidly to the DNA and mixed by vortex followed by 20 min incubation at room temperature prior to use. Final concentration of plasmid DNA in polyplex solution was 20 μg per ml for *in vitro* and 200 μg per ml for *in vivo* experiments. Prepared targeted and non-targeted polyplexes had the similar hydrodynamic diameters and ζ-potentials that were measured by Dynamic Light Scattering Methods using a ZetaPALS instrument (Brookhaven Instruments, Holtsville, NY) as described earlier [23].

2.3. Cell culture

Cloudman S91 mouse melanoma cells (clone M3) and the same cell line stably expressing the *H2A-GFP* gene encoding histone H2A and GFP fusion protein under CMV-promoter or rat *NIS* gene under melanoma-specific MIA-promoter of the human melanoma inhibitory activity gene (hMIA), hereafter called M3, M3 H2A-GFP and M3 NIS cells, respectively, were cultured in DMEM/F12 medium supplemented with 10 % fetal bovine serum (both Gibco Invitrogen, Eugene, OR). The medium for M3 H2A-GFP and M3 NIS cells also

NIH-PA Author Manuscript

NIH-PA Author Manuscript

NIH-PA Author Manuscript

contained geneticin (Acros Organics, Pittsburgh, PA) at 400 μg per ml or puromycin (Fisher BioReagents, Pittsburgh, PA) at 0.4 μg per ml, respectively. All cultured cells were grown at 37 °C in a humidified 5 % CO_2 atmosphere.

Stably transfected cell line M3 NIS was obtained using pMIA-NIS mammalian expression vector [26] carrying ORF rNIS under control chimeric melanoma-specific promoter. ClaI-ClaI fragment containing expression cassette 3ET-pMIA-NIS-SVLPA was excised, filled in with Klenow fragment and cloned into lentiviral vector pLVX-Puro (Clontech) in place of the ClaI-XbaI fragment containing pCMV promoter. To obtain viral particles, HEK293T cells were cotransfected with plasmids 3ET-pMIA-NIS-pLVX-Puro, pVSV-G (Clontech) and pCMV-dR8.91 using Lipofectamine® 2000 Reagent (Life Technologies, Carlsbad, CA), according to the manufacturer's recommendation. M3 cells 48 h after lentiviral infection were cultured for two weeks in selective media containing 0.4 μg/mL puromycin. Obtained M3 NIS cell line was subsequently screened by ^{125}I uptake analysis during three weeks.

Stably transfected cell line M3 H2A-GFP was obtained using pCMV-H2A-GFP vector (kindly provided by Dr. Tatiana Soboleva, John Curtin School of Medical Research, Australian National University, Canberra, Australia) and Lipofectamine® 2000 Reagent according to the manufacturer's recommendations. After transfection cells were cultured for two weeks in selective media containing 400 μg/ml geniticin. To obtain the stable cell line, cell sorting flow cytometry was applied. Obtained M3 H2A-GFP cell line was subsequently screened by flow cytometry.

2.4. ^{125}I accumulation in M3 cells transfected with NIS gene

M3 cells were seeded onto 24-well plates, 25 000 cells per well, and cultivated in serum-containing medium for 24 h. The medium was changed and polyplex solutions were added to the cells to final DNA concentration of 0.5 μg per ml. To determine the kinetics of *NIS* expression in transfected cells, after a selected time (6, 12, 18, 24, 36, 48, 62 or 72 h) the cells were washed once with Hanks' balanced salt solution (PanEco, Moscow, Russia), containing 10 mM HEPES, pH 7.4. Afterwards the same solution containing 5.5 mM glucose and 1 μM $Na^{125}I$ (Isotope, Moscow, Russia) with activity of 0.1 μCi was added to the cells, followed by incubation for 1 h. In control wells the cells were incubated in the same solution with 50 μM NaClO4. Then the cells were rapidly rinsed and lysed with 0.5 M NaOH. The cell-associated radioactivity was measured with gamma-counter (RiaGamma 1271, LKB, Sweden). The radioactivity was normalized to the amount of cells counted in the control wells without $^{125}I^-$.

To determine the iodide uptake in relation to the incubation time, M3 cells after 24 hours of incubation with polyplexes were cultured with 0.1 μ]Ci $Na^{125}I$ for 2, 5, 10, 15, 30, 45, 60, 75 and 90 min. Subsequent washing and counting steps were performed as described above.

2.5. Animals

Our experiments were performed on 6- to 8-week-old female DBA/2 mice (Stolbovaya, Moscow Region, Russia). The animals were maintained under specific pathogen-free conditions with access to mouse chow and water *ad libitum*. The experimental protocol was approved by the Institute Commission for Animals.

2.6. Imaging and analysis of polyplex microdistribution in murine melanoma tumor and normal subcutaneous tissues

2.6.1. Dorsal skinfold chamber implantation and establishment of melanoma tumors—Dorsal skinfold chamber (DSC) consisting of two titanium plates (Irola Verwaltungs Gmbh, Freiburg, Germany) was surgically implanted according to Erten *et al.* |

NIH-PA Author Manuscript

NIH-PA Author Manuscript

NIH-PA Author Manuscript

27|. During the procedure, the animals were anesthetized by intraperitoneal injection of 320 mg per kg of avertin in Hanks' solution. Three days later 5×10^5 of M3 cells in 1 μl of PBS were injected into the space between intact skin and the glass window of DSC using 1-μl Hamilton syringe. Tumors reached sufficient for observation volume at the 7-9th day after inoculation.

2.6.2. Intravital confocal microscopy—Accumulation and microdistribution of QD605-labeled polyplexes in tumor and normal subcutaneous tissues were studied using intravital confocal laser scanning microscopy. Mice were anesthetized using 1 % isoflurane (Abbott Laboratories Ltd, UK) and then given an intravenous injection of 0.4 mg 150 kDa FITC-dextran (Sigma, St. Louis, MO) in 100 μl of PBS for visualization of vessels. Immediately after that, targeted or non-targeted polyplexes, containing 80 μg of QD605-labeled plasmid DNA were injected intravenously. Areas of 450 × 450 μm in subcutaneous or tumor tissue were chosen for analysis using Zeiss LSM 510 META NLO (Carl Zeiss, Oberkochen, Germany) confocal laser scanning microscope equipped with Plan-NEOFLUAR ×10/0.30 lens. Images were obtained using multi-track Z-stack mode (10-12 optical sections for every stack with 8 μm step) at 15, 30, 45, 60, 90, 120, 180 and 240 min after polyplex administration. QD605 were registered using 2-photon excitation at 890 nm and 591 – 612 nm pass band for emission. Blood vessels stained with FITC-dextran were visualized by an argon laser at λ_{ex} = 488 nm and 500 – 550 nm pass band for emission. Background images were captured before polyplex injection.

2.6.3. Analysis of polyplex microdistribution—Obtained images were analyzed using Image-Pro PLUS 5.0 software (Media Cybernetics Inc., Silver Spring, MD). For evaluation of polyplex circulation time in the bloodstream and polyplex pharmacokinetics in tumor or normal subcutaneous tissues including vessels, summarized voxel volumes in QD605 channel (after autofluorescence subtraction) were calculated and normalized to the chosen volumes of the corresponding tissues for each time point. Thus, polyplex concentration was evaluated in voxel volumes per mm^3 of tissue by analogy with [25, 28]. For analysis of polyplex extravasation and microdistribution in tumor or normal subcutaneous tissue, pixel areas of fluorescent objects in QD605 channel (after autofluorescence subtraction) on the vessel wall surface defined by FITC staining and different distances (0-4, 4-8, 8-12, 12-16 and 16-20 μm) from it in the depth of tissue were calculated and normalized to the total areas around chosen vessels (including lumens of these vessels) for each time point. We found significant linear correlation $r > 0.996$ ($p < 0.001$) between these units and the summarized voxel volumes in the same channel per mm^3 of tissue including vessels (Suppl. Fig. 1), that were defined earlier. On the next step, ^{3} calculated pixel areas were converted into voxel volumes per mm of tissue by multiplying by proportionality coefficient that was calculated using the previously obtained correlation. Thus, concentrations of polyplexes in the blood-stream, on the vessel wall surface and inside tumor or normal subcutaneous tissue were defined in the same units of voxel volumes per mm^3 of tissue.

2.7. NIS gene transfer and SPECT/CT imaging—M3 or M3 NIS mouse melanoma tumors were established in female DBA/2 mice by subcutaneous injection of 2×10^6 cells suspended in 20 μl DMEM/F12 media into the flank region. The experiments were started when tumors had reached a tumor volume of 200 mm^3 after 10-days pretreatment with L-thyroxine (Berlin-Chemie, Berlin, Germany) (5 mg/l) in their drinking water to maximally reduce iodide accumulation in thyroid [22]. 12, 24 or 48 hours after intravenous administration of targeted or non-targeted polyplexes (80 μg DNA per mouse), animals (5 mice per group) were anesthetized using 1 % isoflurane and then injected intravenously with 19 MBq of ^{123}I (FSUE Federal center of nuclear medicine projects design and development, Moscow, Russia), followed by monitoring of radioiodine biodistribution on U-SPECT-II/CT

NIH-PA Author Manuscript

NIH-PA Author Manuscript

NIH-PA Author Manuscript

(MiLabs, Utrecht, the Netherlands) scanner during almost 3 hours (13 time frames of 10 min each) using 1.0-mm-diameter pinhole collimator tube. Obtained images were reconstructed merging the last 6 timeframes. For X-ray computer tomography (CT) the accurate scanning mode (2 frames of 7.5 min) was chosen. Quantitative analysis of images after 3D-reconstruction was performed using PMOD 3.4 software (PMOD Technologies Ltd., Switzerland).

2.8. Statistical analysis

All experiments were performed at least in triplicate. Error bars represent SE or SD as indicated in the legends. Between-group differences were analyzed using one-way ANOVA followed by a post hoc Dunnett's t-test. A value of $p < 0.05$ was considered to be significant.

3. Results and discussion

3.1. In vitro NIS gene transfer

Transfection of M3 murine melanoma cells with non-targeted polyplexes containing pCMV-NIS plasmid and following incubation with ^{125}I led to fast iodide uptake by the cells ($\tau_{½}$ = 9 mm) (Fig. 1a). We also 125 evaluated kinetics of *NIS* expression in M3 cells by measuring accumulated ^{125}I radioactivity up to 72 hours after polyplex-mediated transfection. *NIS* expression increased with time and reached the maximal rate at 48 hours (Fig. 1b). M3 cells transfected with targeted polyplexes showed 2-fold higher ^{125}I accumulation in comparison with cells transfected with non-targeted polyplexes. Iodide uptake in transfected cells was blocked by addition of sodium perchlorate, a specific inhibitor of NIS (Fig. 1c). Thus, we confinned feasibility of using *NIS* as a reporter gene along with the advantage of MClSP-targeted polyplexes for *in vitro* gene transfer over non-targeted ones.

3.2. Polyplex accumulation, extravasation and penetration in murine melanoma tumor and normal subcutaneous tissue

3.2.1. Uptake characteristics of targeted polyplexes in tumor and normal subcutaneous tissue—The transport of gene carriers in living organism is the multistep process including circulation within a blood vessel, extravasation with subsequent diffusion in tumor interstitial space, adhesion on the cell surface, uptake and intracellular transport of DNA into the nuclei of cancer cells [29]. Quantitative investigation of the dynamics of such delivery is crucial in enabling the development of more effective gene delivery systems. First of all, we have investigated uptake kinetics of targeted quantum QD605-labeled polyplexes in normal subcutaneous and subcutaneous M3 melanoma tumor tissue (including vessels) of syngeneic DBA/2 mice after intravenous administration. For this purpose, we used DSC [30] and intravital confocal microscopy applied for studies of both tumor vascularization [31] and microdistribution of fluorescently labeled macromolecules [32]. Polyplex concentration was defined as summarized “voxel volume” in QD605 channel normalized to the tissue volume of interest after subtraction of preliminary measured background level. We observed very fast accumulation with subsequent 75 % decrease in concentration of polyplexes in tumor from 15 min up to 4 hours after intravenous administration as well as in normal subcutaneous tissue (Fig. 2). However, the difference in polyplex concentration between tumor and subcutaneous tissues including blood vessels was more than 10 times at 4 hours post-injection. We also evaluated circulation time of polyplexes in the blood-stream which is an important characteristic affecting transfection efficiency *in vivo* [33]. Intravital confocal microscopy in combination with DSC makes it possible to calculate concentration of fluorescently labeled nanoparticles with time in blood to a high degree of accuracy [34]. Polyplex concentration was determined inside collecting venules (30-40 μm in width) or tumor vessels (30-80 μm in width) that were visualized using FITC-dextran in the same way as mentioned above. Polyplex circulation half-time was

NIH-PA Author Manuscript

NIH-PA Author Manuscript

NIH-PA Author Manuscript

estimated to be *ca.* 18 min (Fig. 2). Perhaps, increase in circulation time of polyplexes may improve the EPR effect [35], thus probably increasing their tumor accumulation.

3.2.2. Detailed analysis of polyplex microdistribution—Co-localization of QD605-labeled polyplexes with FITC-dextran-labeled blood vessels showed that the major part of "in tumor-accumulated" polyplexes retained on vessel wall surface as well as in normal subcutaneous tissue (Fig. 3). Significant part of polyplexes in tumor formed large aggregates on the vessel wall surface, but not in the blood-stream. In normal subcutaneous tissue the amount of bound to the vessel wall polyplexes and large polyplex aggregates was significantly less (Fig. 3). The mechanisms by which cationic nanoparticles selectively target tumor endothelium are still hypothetical. This observation may in part result from essential structural and functional distinctions between tumor and normal capillaries. The vessel wall structure is composed of a single layer of endothelial cells lining microvessels surrounded by a basement membrane which contains negatively charged polysaccharides, especially hyaluronan [36]. Tumor vessel walls have large openings between defective endothelial cells where basement membrane matrix may contact with blood [3, 4]. Interaction of hyaluronan or other negatively charged components of basement membrane matrix with positively charged polyplexes in tumor vessels probably may result in enhanced binding and formation of aggregates in contrast to normal subcutaneous tissue where basement membrane is isolated with layer of endothelium with small fenestrations. Moreover, preferential retaining of cationic nanoparticles in tumor vessels occurs presumably due to charge-dependent binding and uptake by a potentially altered glycocalyx of tumor endothelium [37]. There are also mosaic vessels in solid tumors where both endothelial cells and cancer cells form the luminal surface [38]. Recently, it was shown that MC1R overexpression in melanoma cells enhanced the synthesis of syndecan-2, a cell surface heparan sulfate proteoglycan [39]. Therefore, the presence of negatively charged areas due to syndecan-2 overexpression in mosaic vessels of melanoma tumor may also enhance polyplex binding. Anyway, this question requires further investigation.

Subsequent elimination of bound to the vessel wall polyplexes and large polyplex aggregates with time occurred in tumor (Fig. 3, 4a) as well as in normal subcutaneous tissue (Fig. 3, 4b). Perhaps this is owing to the polyplex unpacking on the endothelial cell surface and subsequent release of QD605-labeled DNA into the blood stream. It also may be due to opsonization with plasma proteins [40, 41] and uptake by phagocytic cells [41]. At last, elimination of bound to the vessel wall polyplexes could be explained by polyplex recycling [42, 43, 44] from the lining cells after endocytosis.

In tumor only a part of primarily bound to the vessel wall surface polyplexes was extravasated and penetrated into the tumor tissue. About 60 % of this amount was extravasated during the first 15 minutes post-injection. The limited extravasation of polyplexes in tumor indicates the presence of extravasation barrier caused by high cell and extracellular matrix density, and high intratumoral fluid pressure. At the same time in normal subcutaneous tissue, amount of extravasated polyplexes was 400 times less than in tumor tissue (Fig. 4a, b). It is a striking illustration of the EPR effect in the considered tumor model.

In order to quantify polyplex extravasation and accumulation in tumor or normal subcutaneous tissues, we have developed the mathematical model (see Supplementary Data and Suppl. Fig. 2) which describes kinetics of polyplex clearance, adhesion on vessel wall surface and extravasation processes. Calculations made on the basis of developed kinetics models resulted in one-order higher values of the polyplex binding to the vessel wall surface rate constant (Suppl. Table. 1) that confirms our assumption about structural differences which determine binding affinity for polyplexes. Defined dissociation rate constants of

NIH-PA Author Manuscript

NIH-PA Author Manuscript

NIH-PA Author Manuscript

polyplexes from the vessel wall in both tumor and normal subcutaneous tissues were almost equal (Suppl. Table. 1). This fact indicates similarity of mechanisms of polyplex elimination from the tumor and normal tissues. Mathematical modeling also resulted in two-order higher values of the polyplex extravasation rate constant (Suppl. Table. 1). Thus, pathophysiological irregularities in tumor vasculature provide faster binding and enhanced permeability into tumor tissue in comparison with subcutaneous ones.

3.2.3. Impact of the ligand targeting on polyplex extravasation and penetration deep into tissue—Using intravital microscopy in combination with DSC we have also evaluated the impact of the ligand targeting of polyplexes with MC1SP-peptide on their accumulation, extravasation and penetration into the tumor tissue. We did not revealed any differences in accumulation and extravasation kinetics in tumor between targeted polyplexes and non-targeted ones (Fig. 4b). Therefore, targeting of polyplexes with the specific ligand did not improve their penetration into tumor tissues. It could be explained by primarily passive way of accumulation due to EPR effect. The similar results were obtained also for other nanocarriers after incorporating ligands for specific binding to cancer cells [45, 46]. However, attachment of a ligand to overexpressed receptors on the cancer cell surface to nanoparticles may increase cellular uptake of these vehicles [47]. It was also shown that targeting of polyplexes with a ligand to EGFR [48], or melanocortin-1 receptors [23] resulted in faster cellular accumulation via receptor-mediated endocytosis and enhanced transfection efficacy. Thus, faster cellular uptake is an important condition in terms of successful gene delivery.

For analysis of polyplex penetration into the tumor and normal subcutaneous tissues, quantitative distributions were plotted in dependence of distance from the vessel wall and post-injection time (Fig. 5). According to our data, the maximal distance of polyplex penetration into the tumor tissue (Fig. 5a and b) was about 20 μm. About 40 % of extravasated polyplexes stopped up to 4 μm from the vessel wall, about 90 % — up to 12 μm. In contrast, in normal subcutaneous tissues polyplexes penetrated less than 3 μm from the vessel walls (Fig. 5c). Visualization of microvessels with FITC-dextran in M3 H2A-GFP tumor with nuclear localization of histone H2A and GFP fusion protein identified that the nearest cancer cell nuclei are located from 1 up to 6-7 μm from the vessel wall (Suppl. Fig. 3). Therefore, extravasated polyplexes can reach the nuclei of cancer cells.

There were no differences between targeted and non-targeted polyplexes microdistribution kinetics across the tumor tissue, though targeting of macromolecules or nanoparticles with a ligand can lead to arising of “binding site barrier” *in vivo* [49] limiting penetration of targeted polyplexes. This phenomenon is due to the fact that penetration of ligand-containing macromolecules into tumors could be prevented by their strong binding to target cells possessing receptors/determinants for the ligands. The effect of binding site barrier had been firstly revealed for antibodies [50] as well as for targeted polymeric particles [46]. We did not observe the effect of “binding site barrier” for the both types of our polyplexes probably due to their big hydrodynamic diameters (41.2 ± 4.0 and 43.5 ± 4.7 nm for targeted and non-targeted ones, respectively) which could hamper diffusion of the both types of polyplexes. For instance, according to Lee *et al.* (2010) [46], the effect of “binding site barrier” was observed only with 25 nm-sized nanoparticles but not with 60 nm ones indicating dependence of tissue penetration on particles’ size. The next factor responsible for impeded diffusion of macromolecules (including polyplexes) is negatively charged basement membrane of endothelium [36], extracellular matrix [51] or melanoma cancer cells surface [39]. The point is that many of the solid tumors have increased content of glycosaminoglycans and especially hyaluronan [52, 53]. Our targeted polyplexes as well as non-targeted ones have positive zeta-potentials (22.7 ± 1.0 and 19.4 ± 0.5 mV for targeted

NIH-PA Author Manuscript

NIH-PA Author Manuscript

NIH-PA Author Manuscript

and non-targeted polyplexes, respectively) that also could decrease extravasation and penetration into tumor tissue [54].

3.3. SPECT/CT imaging of ^{123}I accumulation in tumor after NIS gene transfer

To investigate the efficacy of *NIS* gene transfer into murine M3 melanoma tumor in whole, we applied single-photon emission computed tomography (SPECT) as one of the most often clinically used method to visualize accumulation of radiotracers in certain tissues [55]. To find the optimal conditions of tumor imaging in tumor-bearing mice after polyplex-mediated transfection with *NIS,* we evaluated radioactivity accumulation kinetics in M3 NIS tumor with stable *NIS* transfection. The measurements showed that radioactivity accumulation reached a plateau at 90 min after radioiodine intravenous injection that retained for at least 3 hours post-injection (Suppl. Fig. 4). On the next step we studied kinetics of polyplex-mediated transgene expression measured by ^{123}I accumulation in tumor at preset time after administration of targeted polyplexes. According to our data, the maximum of ^{123}I accumulation in tumor was obtained at 24 hours after polyplex injection and reached 6.8 ± 1.1 % ID/g that made it possible to visualize the tumor (Fig. 6a, b, c see also Supplemental Video). The similar kinetics of *NIS* expression in tumor transfected with polyplexes based on polypropylenimine dendrimers was revealed by Chisholm *et al.* (2009) [21]. Thus, our results in compliance with Chisholm's data both confirm transient nature of gene transfer using polymer-based vectors. In non-transfected control group and in the group injected with the targeted polyplexes containing plasmid without promoter, accumulated dose in tumor was about 2.4 ± 0.4 and 2.8 ± 0.3 % ID/g (Fig. 6d). In spite of indistinguishabilities between targeted and non-targeted polyplexes' accumulation and tumor microdistribution (see above), we observed a 2-fold increase in I accumulation in tumor transfected with PEI-PEG-MC1SP polyplexes compared to tumor transfected with PEI-PEG ones (Fig. 6d). This phenomenon could be explained by mechanisms of cell penetration, intracellular trafficking, and polyplex unpacking of these types of polyplexes that strongly determine transfection efficacy. According to our earlier experimental data [23], the difference in transfection efficacy between targeted and non-targeted polyplexes was caused by different rates of intracellular accumulation of packed polyplex nanoparticles. It was shown [56] that receptor-mediated endocytosis occurs faster than unspecific adsorptive one. Our data revealed a significant contribution of the clathrin-dependent receptor-mediated endocytosis pathway for internalization of the targeted polyplexes that provides fast accumulation of polyplex nanoparticles inside target cells [23] and probably diminishes the interaction of the polyplexes with surface proteoglycans that can lead to polyplex unpacking [57] and subsequent degradation in acidic compartments. Polyplex targeting with a specific ligand resulting in fast uptake may overcome so-called "PEG-dilemma" [58]. PEG-dilemma is a contradictory effect of PEGylation enabling to diminish unspecific interactions with blood components, but also reducing cellular uptake and transfection [59]. Therefore, the faster cellular uptake for polyplexes provided by inclusion of a ligand into polymeric part is preferred for successful gene transfer.

Injection of targeted polyplexes resulted in 6.8 ± 1.1 % ID/g in tumor after 24 hours that was 3.5-fold less than maximally achievable level of isotope accumulation that was observed in M3 NIS tumor with permanent *NIS* transfection (24.3 ± 3.5 % ID/g). Most probably this effect was caused by limited extravasation and penetration of polyplexes into the tumor tissue. Perhaps, polyplexes-mediated gene transfer occurs predominantly to areas adjacent to functional tumor blood microvessels as was obtained for lipid nanoparticle-based delivery system that transported siRNA [60].

NIH-PA Author Manuscript

NIH-PA Author Manuscript

NIH-PA Author Manuscript

4. Conclusions

Here, we have investigated the tumor uptake and intravital microdistribution of intravenously administered quantum dot-labeled polyplexes using dorsal skinfold chamber and intravital microscopy that made it possible to identify the EPR effect in comparison with normal subcutaneous tissue. At the same time, only the minor part of accumulated in tumor polyplexes was extravasated followed by a nearby penetration into tumor tissue. There were no differences in histological microdistribution across the melanoma tumor tissue with time between targeted and non-targeted polyplexes. However, according to our previous data targeted polyplexes are more effective in terms of cellular uptake and intracellular trafficking compared to non-targeted ones that could explain enhanced radioiodine accumulation in tumor after *NIS* gene transfer and therefore more pronounced targeting of small melanoma tumors by targeted than by non-targeted polyplexes.

Supplementary Material

Refer to Web version on PubMed Central for supplementary material.

Acknowledgments

Experiments were carried out with the use of the equipment from the Center of collective usage of the Russian Academy of Sciences. This work was supported by Russian Federation State contracts nos. 16.512.12.2002, 13411.100.8799.13.135, and 11411.1008700.13.084, the Russian Foundation for Basic Research grant no. 13-04-01282-a, as well as by NIH grant P50 NS20023. This work was supported in part by M.V. Lomonosov Moscow State University Program of Development. We are also grateful to Dr. T. Soboleva (John Curtin School of Medical Research, Australian National University, Canberra, Australia) for providing with pCMV-H2A-GFP vector, and Dr. V.A. Nikitin (Institute of Cell Biophysics of the RAS) for provided equipment for mouse immobilization during intravital microscopy.

References

1. Iyer AK, Khaled G, Fang J, Maeda H. Exploiting the enhanced permeability and retention effect for tumor targeting. Drug Discov Today. 2006; 11:812–8. [PubMed: 16935749]
2. Yuan F, Dellian M, Fukumura D, Leunig M, Berk DA, Torchilin VP, et al. Vascular permeability in a human tumor xenograft: molecular size dependence and cutoff size. Cancer Res. 1995; 55:3752–6. [PubMed: 7641188]
3. Hashizume H, Baluk P, Morikawa S, McLean JW, Thurston G, Roberge S, et al. Openings between defective endothelial cells explain tumor vessel leakiness. Am J Pathol. 2000; 156:1363–1380. [PubMed: 10751361]
4. Hobbs SK, Monsky WL, Yuan F, Roberts WG, Griffith L, Torchilin VP, et al. Regulation of transport pathways in tumor vessels: role of tumor type and microenvironment. Proc Natl Acad Sci USA. 1998; 95:4607–12. [PubMed: 9539785]
5. Sarin H. Physiologic upper limits of pore size of different blood capillary types and another perspective on the dual pore theory of microvascular permeability. J Angiogenes Res. 2010; 2:14. [PubMed: 20701757]
6. Mehra NK, Mishra V, Jain NK. Receptor-based targeting of therapeutics. Ther Deliv. 2013; 4:369–94. [PubMed: 23442082]
7. Holgado MA, Martin-Banderas L, Alvarez-Fuentes J, Fernandez-Arevalo M, Arias JL. Drug targeting to cancer by nanoparticles surface functionalized with special biomolecules. Curr Med Chem. 2012; 19:3188–95. [PubMed: 22612702]
8. Larson N, Ghandehari H. Polymeric conjugates for drug delivery. Chem Mater. 2012; 24:840–53. [PubMed: 22707853]
9. Ng QK, Sutton MK, Soonsawad P, Xing L, Cheng H, Segura T. Engineering clustered ligand binding into nonviral vectors: alphavbeta3 targeting as an example. Mol Ther. 2009; 17:828–36. [PubMed: 19240693]

NIH-PA Author Manuscript

NIH-PA Author Manuscript

NIH-PA Author Manuscript

10. de Bruin K, Ruthardt N, von Gersdorff K, Bausinger R, Wagner E, Ogris M, et al. Cellular dynamics of EGF receptor-targeted synthetic viruses. Mol Ther. 2007; 15:1297–305. [PubMed: 17457321]
11. Kursa M, Walker GF, Roessler V, Ogris M, Roedl W, Kircheis R, et al. Novel shielded transferrin-polyethylene glycol-polyethylenimine/DNA complexes for systemic tumor-targeted gene transfer. Bioconjug Chem. 2003; 14:222–31. [PubMed: 12526712]
12. Cheng H, Zhu JL, Zeng X, Jing Y, Zhang XZ, Zhuo RX. Targeted gene delivery mediated by folate-polyethylenimine-block-poly(ethylene glycol) with receptor selectivity. Bioconjug Chem. 2009; 20:481–87. [PubMed: 19191579]
13. Danquah MK, Zhang XA, Mahato RI. Extravasation of polymeric nanomedicines across tumor vasculature. Adv Drug Deliv Rev. 2011; 63:623–39. [PubMed: 21144874]
14. Maeda H, Nakamura H, Fang J. The EPR effect for macromolecular drug delivery to solid tumors: Improvement of tumor uptake, lowering of systemic toxicity, and distinct tumor imaging in vivo. Adv Drug Deliv Rev. 2013; 65:71–9. [PubMed: 23088862]
15. Nagamitsu A, Greish K, Maeda H. Elevating blood pressure as a strategy to increase tumor targeted delivery of macromolecular drug SMANCS: cases of advanced solid tumors. Jpn J Clin Oncol. 2009; 39:756–66. [PubMed: 19596662]
16. Barton KN, Stricker H, Brown SL, Elshaikh M, Aref I, Lu M, et al. Phase I study of noninvasive imaging of adenovirus-mediated gene expression in the human prostate. Mol Ther. 2008; 16:1761–9. [PubMed: 18714306]
17. Hingorani M, Spitzweg C, Vassaux G, Newbold K, Melcher A, Pandha H, et al. The biology of the sodium iodide symporter and its potential for targeted gene delivery. Curr Cancer Drug Targets. 2010; 10:242–67. [PubMed: 20201784]
18. Ahn BC. Sodium iodide symporter for nuclear molecular imaging and gene therapy: from bedside to bench and back. Theranostics. 2012; 2:392–402. [PubMed: 22539935]
19. Merron A, Peerlinck I, Martin-Duque P, Burnet J, Quintanilla M, Mather S, et al. SPECT/CT imaging of oncolytic adenovirus propagation in tumours in vivo using the Na/I symporter as a reporter gene. Gene Ther. 2007; 14:1731–8. [PubMed: 17960161]
20. Rajecki M, Sarparanta M, Hakkarainen T, Tenhunen M, Diaconu I, Kuhmonen V, et al. SPECT/CT imaging of hNIS-expression after intravenous delivery of an oncolytic adenovirus and 131I. PLoS One. 2012; 7:e32871. [PubMed: 22412937]
21. Chisholm EJ, Vassaux G, Martin-Duque P, Chevre R, Lambert O, Pitard B, et al. Cancer-specific transgene expression mediated by systemic injection of nanoparticles. Cancer Res. 2009; 69:2655–62. [PubMed: 19258509]
22. Klutz K, Willhauck MJ, Dohmen C, Wunderlich N, Knoop K, Zach C, et al. Image-guided tumor-selective radioiodine therapy of liver cancer after systemic nonviral delivery of the sodium iodide symporter gene. Hum Gene Ther. 2011; 22:1563–74. [PubMed: 21851208]
23. Durymanov MO, Beletkaia EA, Ulasov AV, Khramtsov YV, Trusov GA, Rodichenko NS, et al. Subcellular trafficking and transfection efficacy of polyethylenimine-polyethylene glycol polyplex nanoparticles with a ligand to melanocortin receptor-1. J Control Release. 2012; 163:211–9. [PubMed: 22964392]
24. Kuzmin DV, Vinogradova TV, Kopantzev EP, Sverdlov ED. Cre-LoxP Mediated Strong Enhancement of pBIRC5 Promoter Driven Suicide of Cancer Cells with CD/UPRT and Fluorocytosine. Open Gene Ther J. 2010; 3:31–9.
25. Ulasov AV, Khramtsov YV, Trusov GA, Rosenkranz AA, Sverdlov ED, Sobolev AS. Properties of PEI-based polyplex nanoparticles that correlate with their transfection efficacy. Mol Ther. 2011; 19:103–12. [PubMed: 21045811]
26. Rothfels H, Paschen A, Schadendorf D. Evaluation of combined gene regulatory elements for transcriptional targeting of suicide gene expression to malignant melanoma. Exp Dermatol. 2003; 12:799–810. [PubMed: 14714561]
27. Erten A, Wrasidlo W, Scadeng M, Esener S, Hoffman RM, Bouvet M, et al. Magnetic resonance and fluorescence imaging of doxorubicin-loaded nanoparticles using a novel in vivo model. Nanomedicine. 2010; 6:797–807. [PubMed: 20599526]

NIH-PA Author Manuscript

NIH-PA Author Manuscript

NIH-PA Author Manuscript

28. Akita H, Ito R, Khalil IA, Futaki S, Harashima H. Quantitative three-dimensional analysis of the intracellular trafficking of plasmid DNA transfected by a nonviral gene delivery system using confocal laser scanning microscopy. Mol Ther. 2004; 9:443–51. [PubMed: 15006612]
29. Nishikawa M, Huang L. Nonviral vectors in the new millennium: delivery barriers in gene transfer. Hum Gene Ther. 2001; 12:861–70. [PubMed: 11387052]
30. Laschke MW, Vollmar B, Menger MD. The dorsal skinfold chamber: window into the dynamic interaction of biomaterials with their surrounding host tissue. Eur Cell Mater. 2011; 22:147–64. [PubMed: 21932192]
31. Alexander S, Koehl GE, Hirschberg M, Geissler EK, Friedl P. Dynamic imaging of cancer growth and invasion: a modified skin-fold chamber model. Histochem Cell Biol. 2008; 130:1147–54. [PubMed: 18987875]
32. Li L, Ten Hagen TL, Bolkestein M, Gasselhuber A, Yatvin J, van Rhoon GC, et al. Improved intratumoral nanoparticle extravasation and penetration by mild hyperthermia. J Control Release. 2013; 167:130–7. [PubMed: 23391444]
33. Neu M, Germershaus O, Behe M, Kissel T. Bioreversibly crosslinked polyplexes of PEI and high molecular weight PEG show extended circulation times in vivo. J Control Release. 2007; 124:69–80. [PubMed: 17897749]
34. Hori K, Nishihara M, Yokoyama M. Vital microscopic analysis of polymeric micelle extravasation from tumor vessels: macromolecular delivery according to tumor vascular growth stage. J Pharm Sci. 2010; 99:549–62. [PubMed: 19544373]
35. Moghimi SM, Hunter AC, Murray JC. Long-circulating and target-specific nanoparticles: theory to practice. Pharmacol Rev. 2001; 53:283–318. [PubMed: 11356986]
36. Gao F, Okunieff P, Han Z, Ding I, Wang L, Liu W, et al. Hypoxia-induced alterations in hyaluronan and hyaluronidase. Adv Exp Med Biol. 2005; 566:249–56. [PubMed: 16594159]
37. Schmitt-Sody M, Strieth S, Krasnici S, Sauer B, Schulze B, Teifel M, et al. Neovascular targeting therapy: paclitaxel encapsulated in cationic liposomes improves antitumoral efficacy. Clin Cancer Res. 2003; 9:2335–41. [PubMed: 12796403]
38. Chang YS, di Tomaso E, McDonald DM, Jones R, Jain RK, Munn LL. Mosaic blood vessels in tumors: frequency of cancer cells in contact with flowing blood. Proc Natl Acad Sci USA. 2000; 97:14608–13. [PubMed: 11121063]
39. Chung H, Lee JH, Jeong D, Han IO, Oh ES. Melanocortin 1 receptor regulates melanoma cell migration by controlling syndecan-2 expression. J Biol Chem. 2012; 287:19326–35. [PubMed: 22493442]
40. Zhong D, Jiao Y, Zhang Y, Zhang W, Li N, Zuo Q, et al. Effects of the gene carrier polyethyleneimines on structure and function of blood components. Biomaterials. 2013; 34:294–305. [PubMed: 23069714]
41. Owens DE, Peppas NA. Opsonization, biodistribution, and pharmacokinetics of polymeric nanoparticles. Int J Pharm. 2006; 307:93–102. [PubMed: 16303268]
42. Gonçalves C, Mennesson E, Fuchs R, Gorvel JP, Midoux P, Pichon C. Macropinocytosis of polyplexes and recycling of plasmid via the clathrin-dependent pathway impair the transfection efficiency of human hepatocarcinoma cells. Mol Ther. 2004; 10:373–85. [PubMed: 15294184]
43. Mickler FM, Vachutinsky Y, Oba M, Nishiyama N, Kataoka K, Bräuchle C, et al. Effect of integrin targeting and PEG shielding on polyplex micelle internalization studied by live-cell imaging. J Control Release. 2011; 156:364–73. [PubMed: 21843561]
44. Barua S, Rege K. The influence of mediators of intracellular trafficking on transgene expression efficacy of polymer-plasmid DNAcomplexes. Biomaterials. 2010; 31:5894–902. [PubMed: 20452664]
45. Kirpotin DB, Drummond DC, Shao Y, Shalaby MR, Hong K, Nielsen UB, et al. Antibody targeting of long-circulating lipidic nanoparticles does not increase tumor localization but does increase internalization in animal models. Cancer Res. 2006; 66:6732–40. [PubMed: 16818648]
46. Lee H, Fonge H, Hoang B, Reilly RM, Allen C. The effects of particle size and molecular targeting on the intratumoral and subcellular distribution of polymeric nanoparticles. Mol Pharm. 2010; 7:1195–208. [PubMed: 20476759]

NIH-PA Author Manuscript

NIH-PA Author Manuscript

NIH-PA Author Manuscript

47. Kwon IK, Lee SC, Han B, Park K. Analysis on the current status of targeted drug delivery to tumors. J Control Release. 2012; 164:108–14. [PubMed: 22800574]
48. von Gersdorff K, Ogris M, Wagner E. Cryoconserved shielded and EGF receptor targeted DNA polyplexes: cellular mechanisms. Eur J Pharm Biopharm. 2005; 60:279–85. [PubMed: 15939238]
49. Lammers T, Kiessling F, Hennink WE, Storm G. Drug targeting to tumors: principles, pitfalls and (pre-) clinical progress. J Control Release. 2012; 161:175–87. [PubMed: 21945285]
50. Juweid M, Neumann R, Paik C, Perez-Bacete MJ, Sato J, van Osdol W, et al. Micropharmacology of monoclonal antibodies in solid tumors: direct experimental evidence for a binding site barrier. Cancer Res. 1992; 52:5144–53. [PubMed: 1327501]
51. Wiig H, Gyenge C, Iversen PO, Gullberg D, Tenstad O. The role of the extracellular matrix in tissue distribution of macromolecules in normal and pathological tissues: potential therapeutic consequences. Microcirculation. 2008; 15:283–96. [PubMed: 18464158]
52. Rønnov-Jessen L, Petersen OW, Bissell MJ. Cellular changes involved in conversion of normal to malignant breast: importance of the stromal reaction. Physiol Rev. 1996; 76:69–125. [PubMed: 8592733]
53. Toole BP. Hyaluronan: from extracellular glue to pericellular cue. Nat Rev Cancer. 2004; 4:528–39. [PubMed: 15229478]
54. Krasnici S, Werner A, Eichhorn ME, Schmitt-Sody M, Pahernik SA, Sauer B, et al. Effect of the surface charge of liposomes on their uptake by angiogenic tumor vessels. Int J Cancer. 2003; 105:561–7. [PubMed: 12712451]
55. Beekman F, van der Have F. The pinhole: gateway to ultra-high-resolution three-dimensional radionuclide imaging. Eur J Nucl Med Mol Imaging. 2007; 34:151–61. [PubMed: 17143647]
56. Strømhaug PE, Berg TO, Gjøen T, Seglen PO. Differences between fluid-phase endocytosis (pinocytosis) and receptor-mediated endocytosis in isolated rat hepatocytes. Eur J Cell Biol. 1997; 73:28–39. [PubMed: 9174669]
57. Hanzlíková M, Ruponen M, Galli E, Raasmaja A, Aseyev V, Tenhu H, et al. Mechanisms of polyethylenimine-mediated DNA delivery: free carrier helps to overcome the barrier of cell-surface glycosaminoglycans. J Gene Med. 2011; 13:402–9. [PubMed: 21721076]
58. Zhang Y, Satterlee A, Huang L. In vivo gene delivery by nonviral vectors: overcoming hurdles? Mol Ther. 2012; 20:1298–1304. [PubMed: 22525514]
59. Noga M, Edinger D, Kläger R, Wegner SV, Spatz JP, Wagner E, et al. The effect of molar mass and degree of hydroxyethylation on the controlled shielding and deshielding of hydroxyethyl starch-coated polyplexes. Biomaterials. 2013; 34:2530–8. [PubMed: 23312901]
60. Li L, Wang R, Wilcox D, Zhao X, Song J, Lin X, et al. Tumor vasculature is a key determinant for the efficiency of nanoparticle-mediated siRNA delivery. Gene Ther. 2012; 19:775–80. [PubMed: 21956688]

NIH-PA Author Manuscript
NIH-PA Author Manuscript
NIH-PA Author Manuscript

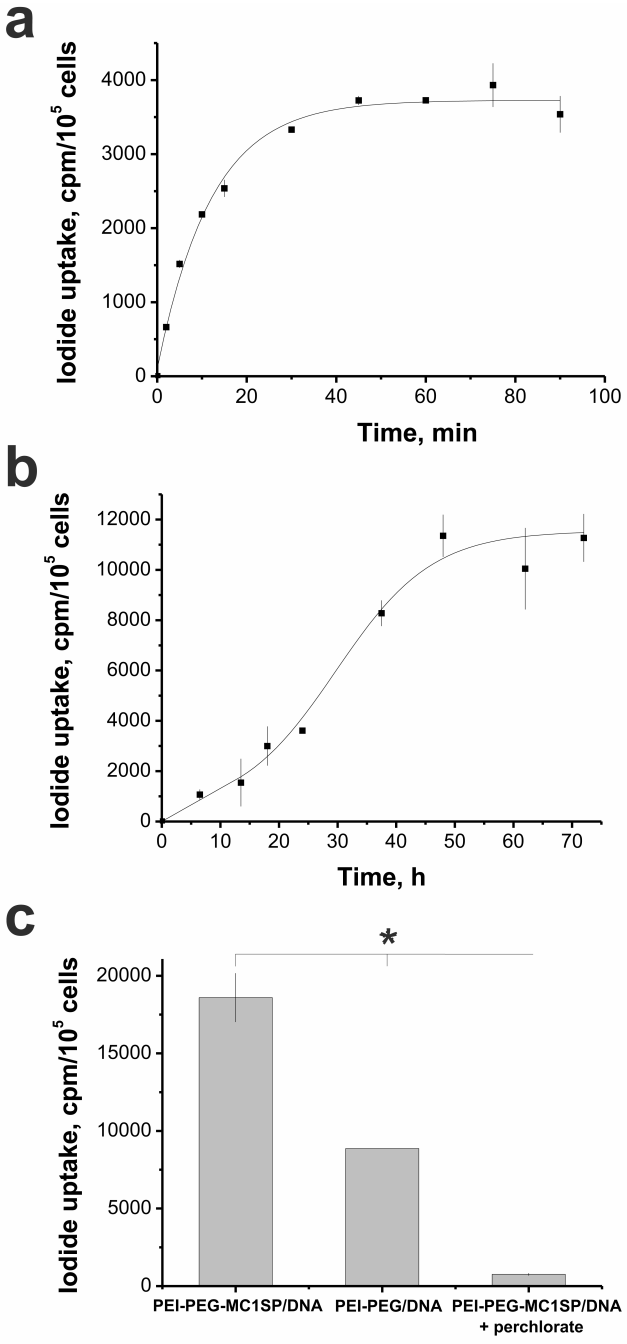

Fig. 1.

In vitro polyplex-mediated *NIS* gene delivery. Uptake kinetics of ^{125}I in murine Cloudman melanoma M3 cells transfected with *NIS* gene after 24 hours of incubation with polyplexes (a) and *NIS* gene expression kinetics in M3 cells transfected with polyplexes and measured by ^{125}I uptake after 1 h of incubation with ^{125}I (b). ^{125}I accumulation in M3 cells at 48 hours after *NIS* transfection and 1 h of incubation with ^{125}I with targeted (PEI-PEG-MC1SP/DNA) and non-targeted (PEI-PEG/DNA) polyplexes as well as block of iodide uptake in transfected cells by addition of sodium perchlorate (c). Values are means ± SD. *$p < 0.001$.

NIH-PA Author Manuscript

NIH-PA Author Manuscript

NIH-PA Author Manuscript

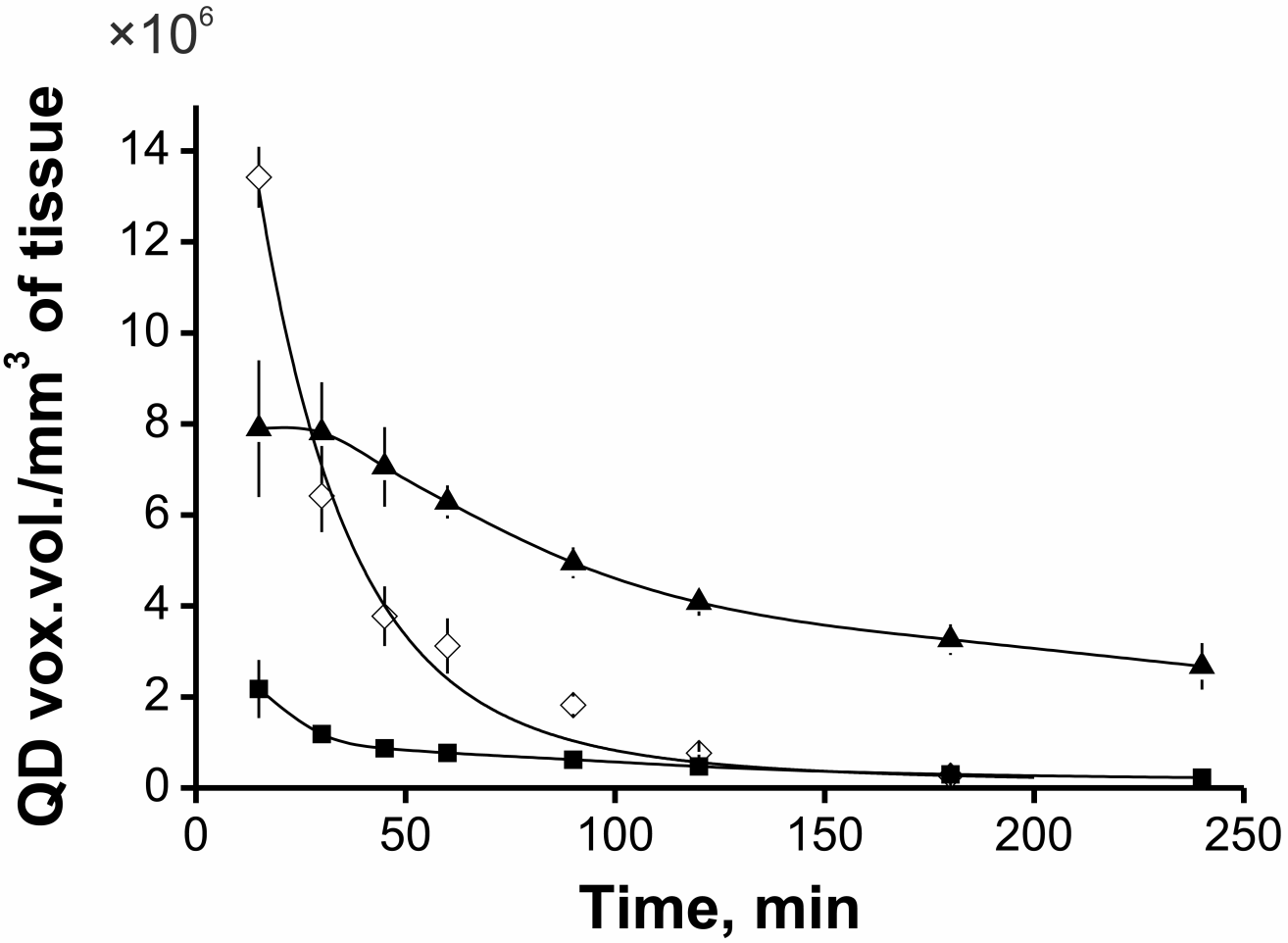

Fig. 2.

Concentration kinetics of targeted polyplexes in the blood-stream (♦), tumor (▲) and normal subcutaneous tissue (■) defined as QD voxel volume per mm^3 of tissue that was determined using confocal intravital microscopy. Polyplexes, containing 80 μg of QD605-labeled plasmid DNA were injected intravenously. Values are means ± SD.

NIH-PA Author Manuscript
NIH-PA Author Manuscript
NIH-PA Author Manuscript

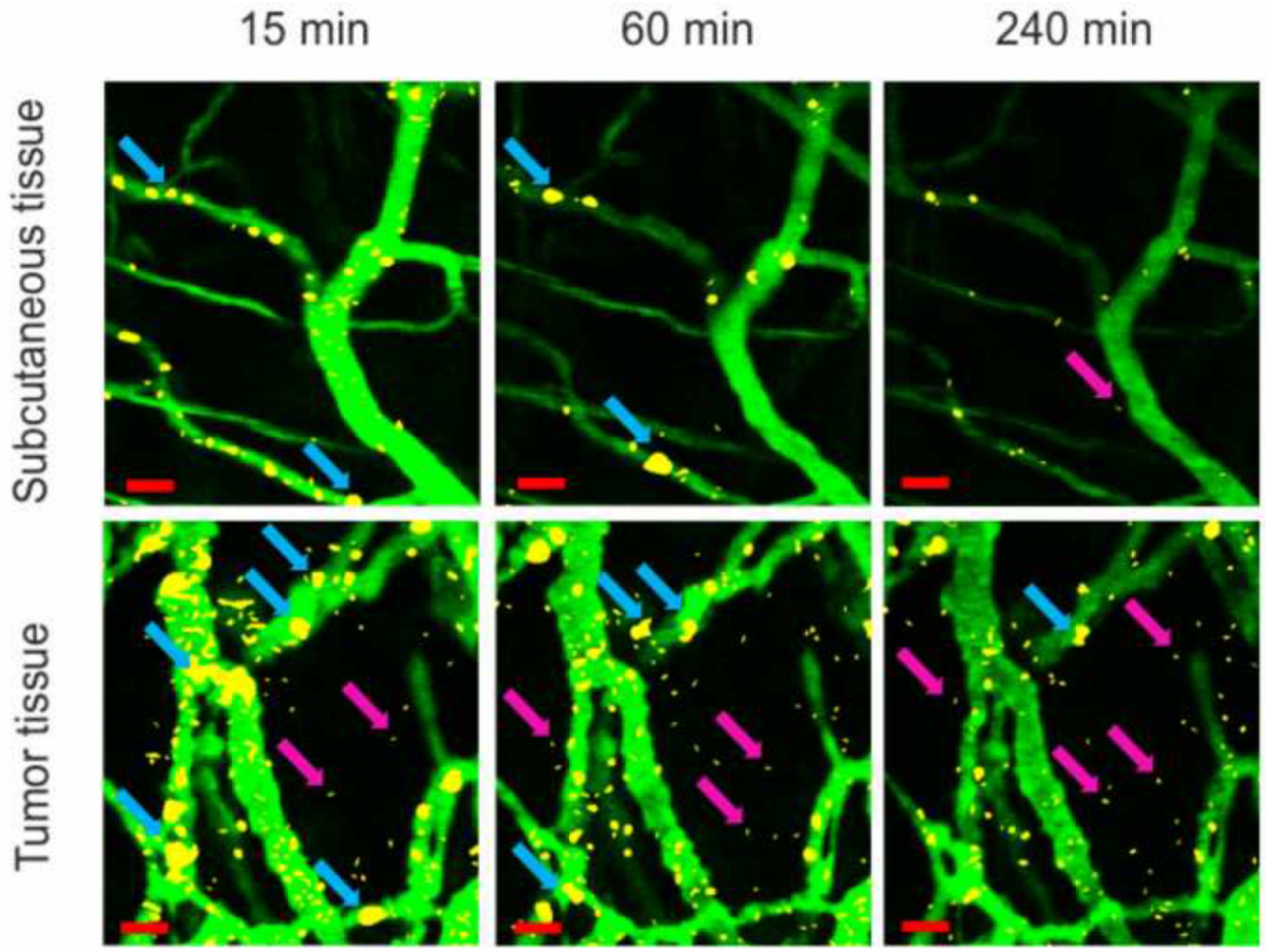

Fig. 3.

Microdistribution of MC1SP-targeted polyplexes in normal subcutaneous (top panel) and tumor (bottom panel) tissues at 15, 60 and 240 min post-injection. Blood vessels were stained by injection of 150 kDa FITC-dextran. Polyplexes, containing 80 μg of QD605-labeled plasmid DNA were administrated intravenously. Images were obtained using intravital confocal microscopy (for details see the Materials and Methods section). Background fluorescence from images captured before polyplex injection was subtracted. Blue arrows indicate large aggregates of polyplexes, purple arrows – extravasated polyplexes. The bars indicate 20 μm.

NIH-PA Author Manuscript

NIH-PA Author Manuscript

NIH-PA Author Manuscript

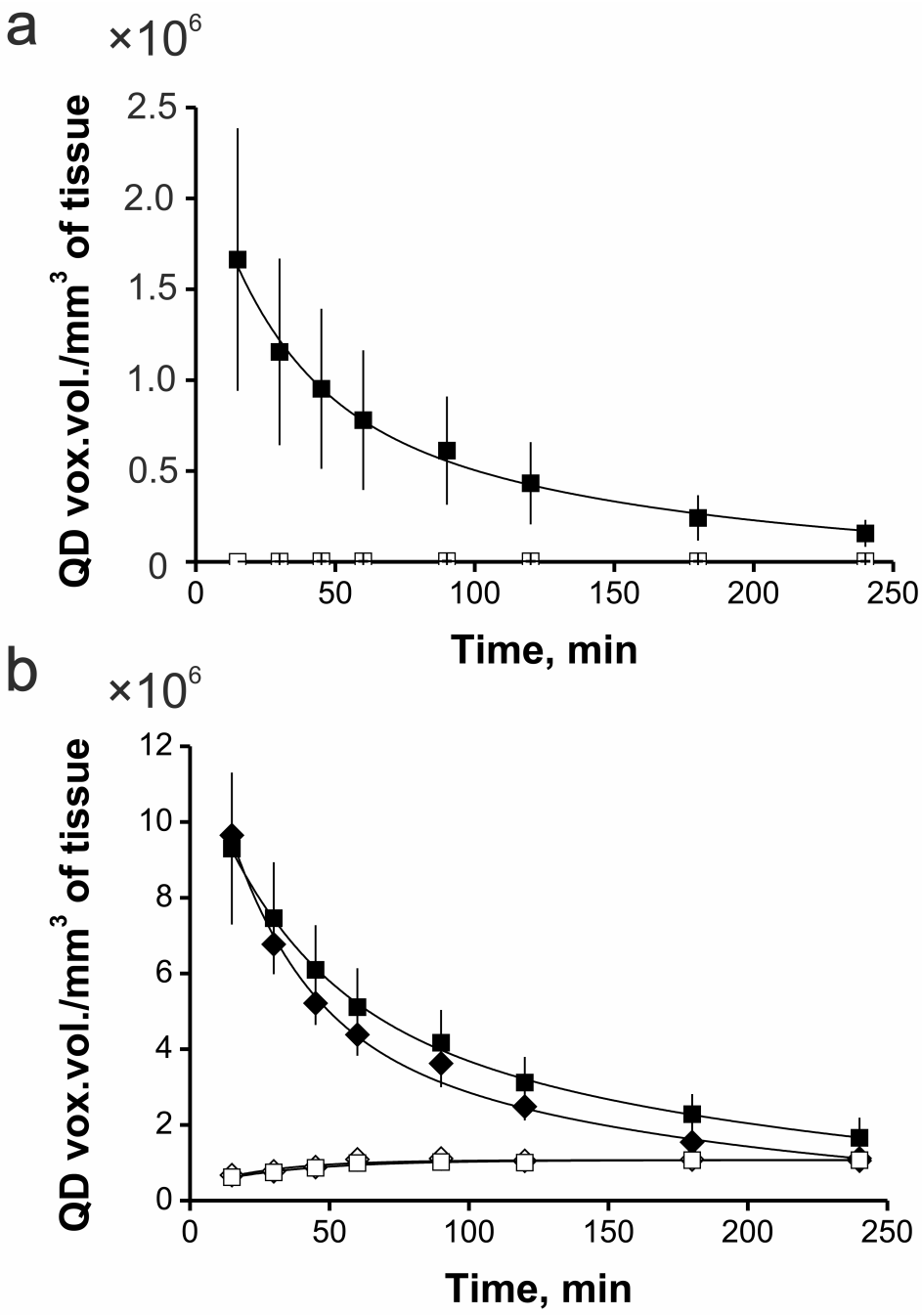

Fig. 4.

Microdistribution kinetics of polyplexes in normal subcutaneous (a) and tumor (b) tissues defined as QD voxel volume of fluorescent objects in QD605 channel (after autofluorescence subtraction) per mm^3 of tissue. Polyplexes, containing 80 μg of QD605-labeled plasmid DNA were administrated intravenously. Blood vessels were stained by injection of 150 kDa FITC-dextran. Subsequent co-localization analysis enabled to detect bound to the vessel wall targeted (■) and non-targeted (◆) polyplexes as well as extravasated targeted (■) and non-targeted (◆) ones. Values are means ± SEM.

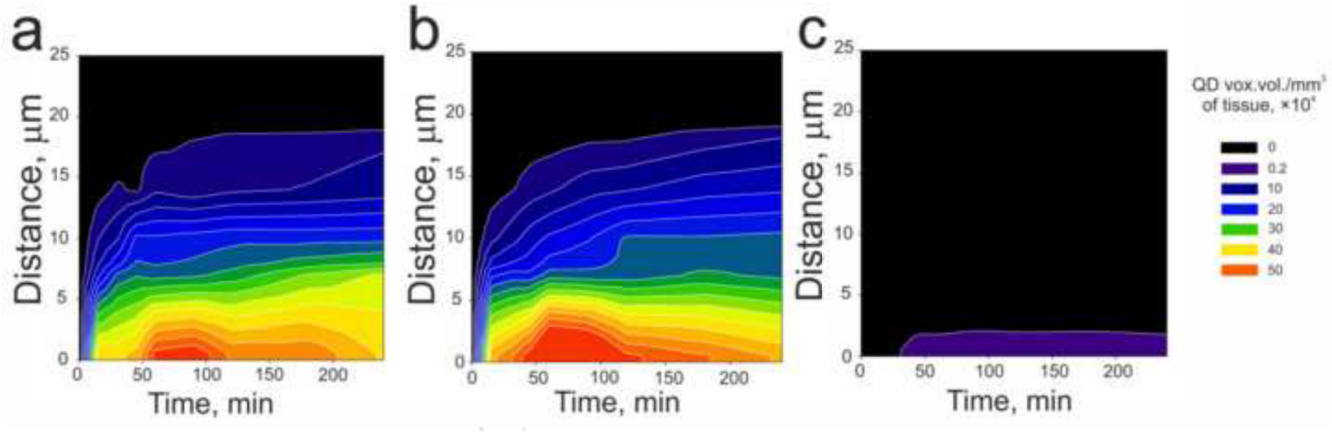

Fig. 5.

Microdistribution kinetics of extravasated MC1SP-targeted (a, c) and non-targeted (b) polyplexes in tumor (a, b) and normal subcutaneous (c) tissues defined as pixel areas of fluorescent objects in QD605 channel (after autofluorescence subtraction) per mm of vessel length. Polyplexes, containing 80 μg of QD605-labeled plasmid DNA were administrated intravenously. Blood vessels were stained by injection of 150 kDa FITC-dextran. Subsequent colocalization analysis made it possible to detect extravasated polyplexes on the different distances from the vessel wall in the depth of tissue.

NIH-PA Author Manuscript
NIH-PA Author Manuscript
NIH-PA Author Manuscript

NIH-PA Author Manuscript
NIH-PA Author Manuscript
NIH-PA Author Manuscript

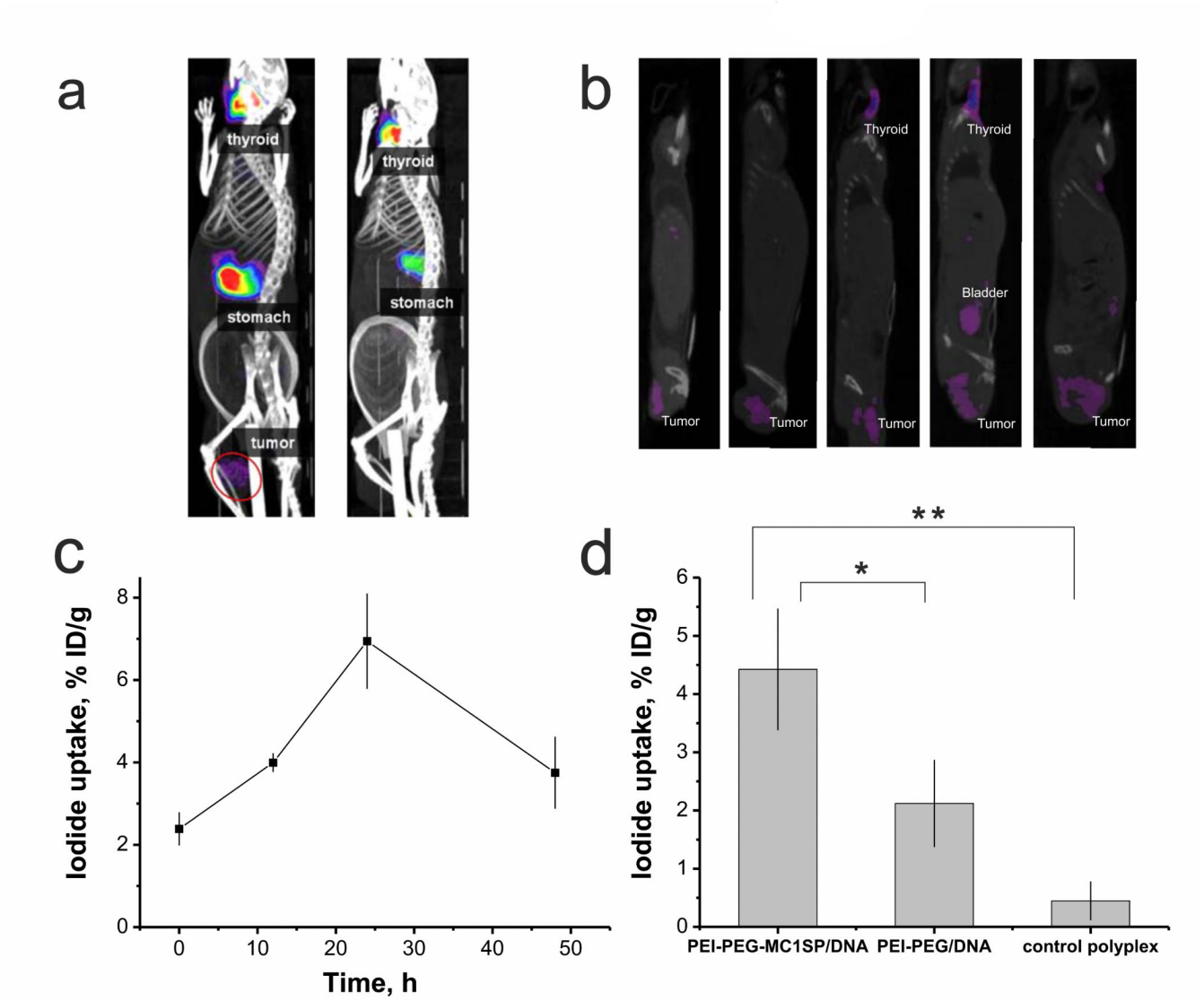

Fig. 6.

SPECT/CT imaging of ^{123}I accumulation in M3 melanoma tumor after *NIS* gene transfer. Reconstructed 3D-projections of mice at 24 h after injection of targeted polyplexes with plasmid DNA encoding *NIS* (left) or targeted polyplexes containing plasmid without promoter as a control (right) (a). Reconstructed images of saggital planes passing through the tumors of five mice at 24 h after injection of targeted polyplexes (b). *NIS* expression with time measured by iodide uptake after intravenous administration of targeted polyplexes, containing 80 μg of plasmid DNA encoding *NIS* (c). ^{123}I accumulation in tumor at 24 h after injection of targeted (PEI-PEG-MC1SP/DNA) polyplexes compared to non-targeted (PEI-PEG/DNA) ones and targeted polyplexes containing plasmid without promoter (control polyplexes) (d). Background level observed in non-transfected control (2.4 ± 0.4 % ID/g) was subtracted in (d). 18.5 MBq of ^{123}I was injected intravenously for visualizing of *NIS* gene expression. All values are means ± SD % ID/g. *$p < 0.001$, **$p < 0.0001$.